Supplementary Information for

SOX9-COL9A3 dependent regulation of choroid plexus epithelial polarity governs blood-cerebrospinal fluid barrier integrity

Authors: Keng Ioi Vong[a], Tsz Ching Ma[a], Baiying Li[a], Thomas Chun Ning Leung[a,c], Wenyan Nong[a], Sai Ming Ngai[a,c,d], Jerome Ho Lam Hui[a,c], Liwen Jiang[a,b,c], Kin Ming Kwan[a,b,c,*]

Author Affiliations: [a] School of Life Sciences, [b] Centre for Cell and Developmental Biology, [c] State Key Laboratory of Agrobiotechnology (CUHK), [d] AoE Centre for Genomic Studies on Plant-Environment Interaction for Sustainable Agriculture and Food Security, The Chinese University of Hong Kong, Hong Kong, P.R. China

*Corresponding author: Kin Ming Kwan
Email: kmkwan@cuhk.edu.hk

This PDF file includes:
Supplementary Methods
Figs. S1 to S12
Tables S1 to S3
SI references

***SI* Materials and Methods**

Histology and immunofluorescence. Brain tissues were fixed in 4% paraformaldehyde
(PFA) overnight and subsequently processed for paraffin embedding and sectioning at 7 µm.
For preparation of cryosections, PFA-fixed tissues were immersed in 20% sucrose followed
by 30% sucrose, embedded in optimal cutting temperature (OCT) compound and sectioned
on a cryostat (Leica CM1950) at 15µm. Fluorescence images were acquired using Olympus
FV1000 or Leica TCS SP8 microscope.

Antibodies. The following primary antibodies were used in this study: rabbit anti-AE2
(#ab42687, Abcam), rabbit anti-albumin (#126584, Calbiochem), rabbit anti-ATP1a1
(#14418-1-AP, Proteintech), rabbit anti-AQP1 (#ab9566, Millipore), rabbit anti-ARL13B
(#ab136648, Abcam), mouse anti-β-catenin (#610153, BD Transduction), rabbit anti-type I
Collagen (#ab34710, Abcam), rabbit anti-CD31 (#ab28364, Abcam), mouse anti-CLDN5
(#187364, Invitrogen), mouse anti-E-cadherin (#610181, BD Transduction), rabbit anti-
laminin (#ab11575, Abcam), rat anti-ITGA6 (#555734, BD Pharmingen), rabbit anti-NKCC1
(#AB59791, Abcam), rabbit anti-PAR3 (#07-330, Millipore), rabbit anti-SOX9 (#AB5535,
Millipore), goat anti-SOX9 (#AF3075, R&D system), mouse anti-transthyretin (#66108-1-IG,
Proteintech), mouse anti-α-tubulin (#05-829, Millipore), mouse anti-acetylated tubulin
(#T7451, Sigma), rabbit anti-ZO-1 (#61-7300, Life Technologies). Alexa-488, Alexa-568 or
Alexa-647-conjugated secondary antibodies were from Life Technologies.

RNA isolation, reverse transcription and qPCR. Total choroid plexus RNA from controls
and *Sox9* CKO mutants were extracted with TRIzol reagent (Life Technologies). cDNA was
prepared using M-MLV Reverse Transcriptase (Life Technologies) with oligonucleotide
dT primers. Real-time quantitative PCR (qPCR) was performed using Power SYBR^{TM} Green
PCR Master Mix (Thermo Fisher) and specific primers listed in *SI Appendix, Table S3* on the
Bio-Rad CFX96 Real-Time PCR Platform. Individual sample was assayed in triplicates.
Gene expression was normalized with β-actin expression.

RNAscope®_Multiplex Fluorescent Assay
RNAscope®_Multiplex Fluorescent Assay on fixed frozen tissue sections was performed
according to the manufacturer's instruction (Advanced Cell Diagnostics). We used
RNAscope_Probe-Mm-Col9a3 (#872461, Advanced Cell Diagnostics) to detect *Col9a3*
expression in the embryonic brain. Immunostaining on RNAscope sections were performed
following manufacturer's protocol. Images were acquired using Leica TCS SP8 microscope.

Transmission electron microscopy (TEM).

Embryonic CP were dissected in ice-cold PBS and immediately frozen in a high-pressure freezer (EM PACT2, Leica), followed by subsequent freeze substitution in dry acetone containing 0.1 % uranyl acetate at –85 °C in AFS freeze-substitution unit (Leica). Infiltration with HM20, embedding, and UV polymerization were performed stepwise at -35 °C. Ultrathin sections were obtained with an ultramicrotome (UC7, Leica). Electron micrographs were captured using a Hitachi H-7650 transmission electron microscope with CCD camera operating at 80 kV.

Chromatin immunoprecipitation (ChIP)-qPCR.

E16.5 CP were dissected, pooled together, dissociated and fixed. Crosslinked chromatin was sheared by sonication for 30 pulses of 20 s at 50 % duty cycle (Branson Sonifier 150). The chromatin was precleared with Protein G-Agarose (Santa Cruz) at 4 °C for 2 h, followed by incubation with anti-SOX9 (8 μg) or control IgG (Invitrogen) at 4 °C overnight. Chromatin was immunoprecipitated with Dynabeads Protein G (Life Technologies) at 4 °C for 2 h. Isolated chromatin was eluted at 65 °C followed by quantitative PCR with primers listed in *SI Appendix,* Table S3.

Microtubule regrowth assay.

Microtubule regrowth assay was carried out with optimization from published protocols (1). Isolated CP tissues were transferred to DMEM and kept on ice for 45 min. Microtubules were then allowed to regrow for 5 min at room temperature, followed by washing in extraction buffers containing 60 mM PIPES, 25 mM HEPES, 10 mM EGTA, 2 mM $MgCl_2$, 0.1% Saponin, 0.25 nM nocodazole and 0.25 nM paclitaxel. The CP was then fixed in ice-cold methanol for 10 min.

Neurosphere culture. Cerebella or dorsal telencephalon from E14.5 mice were digested with 10 U/ml Papain (Worthington Biochemical). Single cell suspension was plated at 1×10^5 cells/6-well in NSC proliferation medium (NeuroCult basal medium with proliferation supplement, Stem Cell Technologies) supplemented with 20 ng/ml epidermal growth factor (EGF; PeproTech). Neurospheres were supplemented with CSF from control or mutants at 1-day *in vitro* and cultured for 7 days. Analyses were performed from at least 15 random views.

CP epithelial primary culture. CP primary culture was performed as previously described with minor modifications (2). CP epithelial cells were isolated from E18.5 CP using Papain dissociation system (Worthington). CP epithelial cells were seeded at 2×10^5 cells per 24-well and cultured in DMEM supplemented with 10 % (v/v) FBS, 2 mM Glutamine, 10 ng/ml EGF,

20 μM Ara-C and 100 U/ml penicillin-streptomycin at 37 °C in 5% CO_2 incubator. For the inhibition of integrin α6 function, CP epithelial cells were incubated with ITGA6-neutralizing antibody with gentle rocking for 20 min at 37 °C prior to seeding onto laminin-coated coverslips.

Embryonic CSF collection

Embryonic CSF was isolated from E17.5 embryos by micro-aspiration (Micro4, World Precision Instrument) using a pulled glass microcapillary pipette inserted into the fourth ventricle. CSF collected for analysis was pooled from 2 or 3 litters. Samples were microscopically inspected for the presence of blood and were discarded if showing signs of contamination. Collected CSF was then centrifuged at 13,000 g for 5 min to remove cell debris and stored at -80 °C

Measurement of CSF total protein level.

CSF samples were thawed on ice. Protein concentration in the CSF was measured using a Pierce Bicinchoninic Acid protein (BCA) assay kit (Thermo Scientific). Colorimetric measurements were performed in triplicate using a NanoDrop 2000c (Thermo Fisher Scientific).

Atomic absorption spectroscopy.

Na^+ and K^+ concentrations in the CSF were measured by flame atomic absorption spectroscopy using a Hitachi Z2300 spectrophotometer.

LC-MS/MS analysis of CSF protein concentrations. 25 μg of each sample was diluted in 20 μl of 500 mM triethylammonium bicarbonate (TEAB) at pH 8.5 with 0.1% SDS. Proteins were reduced with 5 mM tris(2-carboxyethyl) phosphine for 1 h at 60 °C and alkylated with 10 mM methyl methanethiosulfonate for 10 min in dark at room temperature. Then the proteins were digested with sequencing-grade trypsin (Promega) overnight at 37 °C of 1:20 ratio. For labeling, each iTRAQ reagent was dissolved in 70 μl of isopropanol and incubated for 1 h at room temperature with samples, followed by resuspension in 0.1% trifluoroacetic acid and fractionated into 4 fractions with increasing ACN concentrations (7.5%, 12.5%, 17.5%, 50%) using high pH reversed-phase fractionation kit (Thermo Fisher Scientific). 1 μg of iTRAQ labeled peptides was subjected to nano-LC separation using a Dionex UltiMate 3000 RSLC nano system using a 25 cm-long, 75 um-i.d. C18 column. The peptides were eluted from the column at a constant flow rate of 0.3 μl/min with a linear gradient from 2% to 10% of ACN over 3 min and then from 10% to 35% of ACN over 50 min. The eluate was analyzed by an Orbitrap Fusion Lumos Tribrid mass spectrometer (Thermo Fisher Scientific). MS and MS/MS scans were acquired in the Orbitrap with a mass resolution of 120,000 and

15,000 respectively. MS scan range was from 375 to 1500 m/z with AGC target 4e5 and maximum injection time was 50 ms. The AGC target and maximum injection time for MS/MS were 5e4 and 100 ms respectively. HCD mode was used as fragmentation mode with 38% collision energy. Precursor isolation windows were set to 0.7 m/z. Data were analyzed by Proteome Discoverer version 2.3 with SEQUEST as a search engine. Data was searched against UnipProt Mus musculus database. The searching parameters were as follows: iTRAQ4plex of lysine, tyrosine or peptide N-terminus (+144.102 Da), methylthiol of cysteine (+45.988 Da) and oxidation of methionine (+15.9949 Da) was set as dynamic modification; precursor-ion mass tolerance, 10 ppm; fragments-ion mass tolerance, 0.02 Da. Proteins were considered to be differentially expressed if the difference was statistically significant (Benjamini corrected P values < 0.05) and the fold change was > 1.2 or < 0.83. The differentially expressed proteins were subjected to analysis with the DAVID (the Database for Annotation, Visualization, and Integrated Discovery; Version 6.8) programs for annotation enrichment analysis. The enrichment analysis in DAVID was performed based on the "GOTERM_BP_DIRECT", "GOTERM_MF_DIRECT", and "GOTERM_CC_DIRECT" database.

RNA sequencing. Total RNAs were collected from the hindbrain CP of control and *Sox9* CKO mutants at E16.5. Adapters were trimmed and low-quality bases were removed from raw reads using Trimmomatic (version 0.33) as described previously (3). Processed reads were then mapped to mouse reference genome (NCBI build 37.2, ftp://igenome:G3nom3s4u@ussd-ftp.illumina.com/Mus_musculus/NCBI/build37.2/Mus_musculus_NCBI_build37.2.tar.gz)) using TopHat (version 2.1.1) and Cufflinks (version 2.2.1) with all default parameters. Differential gene expressions were evaluated using Cuffdiff (version 2.2.1) (4).
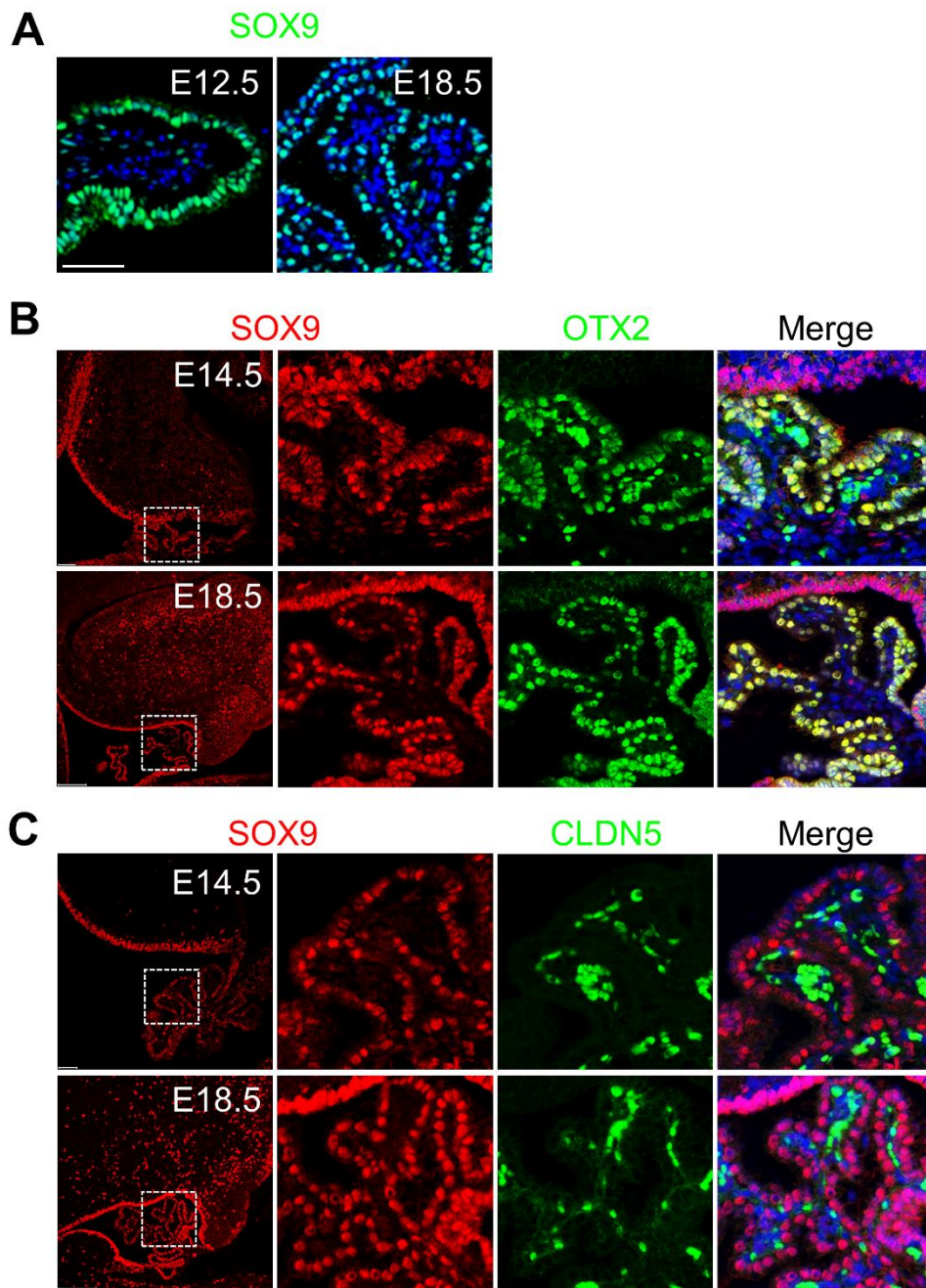
Fig. S1 SOX9 expression in the CP. (A) Immunostaining for SOX9 on coronal section from E12.5 and E18.5 embryos. At both developmental stages, SOX9 was specifically expressed in the CP epithelial cell layer. (B) Double immunostaining for SOX9 and OTX2 at E14.5 and E18.5. (C) Double immunostaining for SOX9 and claudin-5 (CLDN5) at E14.5 and E18.5. Scale bars, 50 μm in A-C.
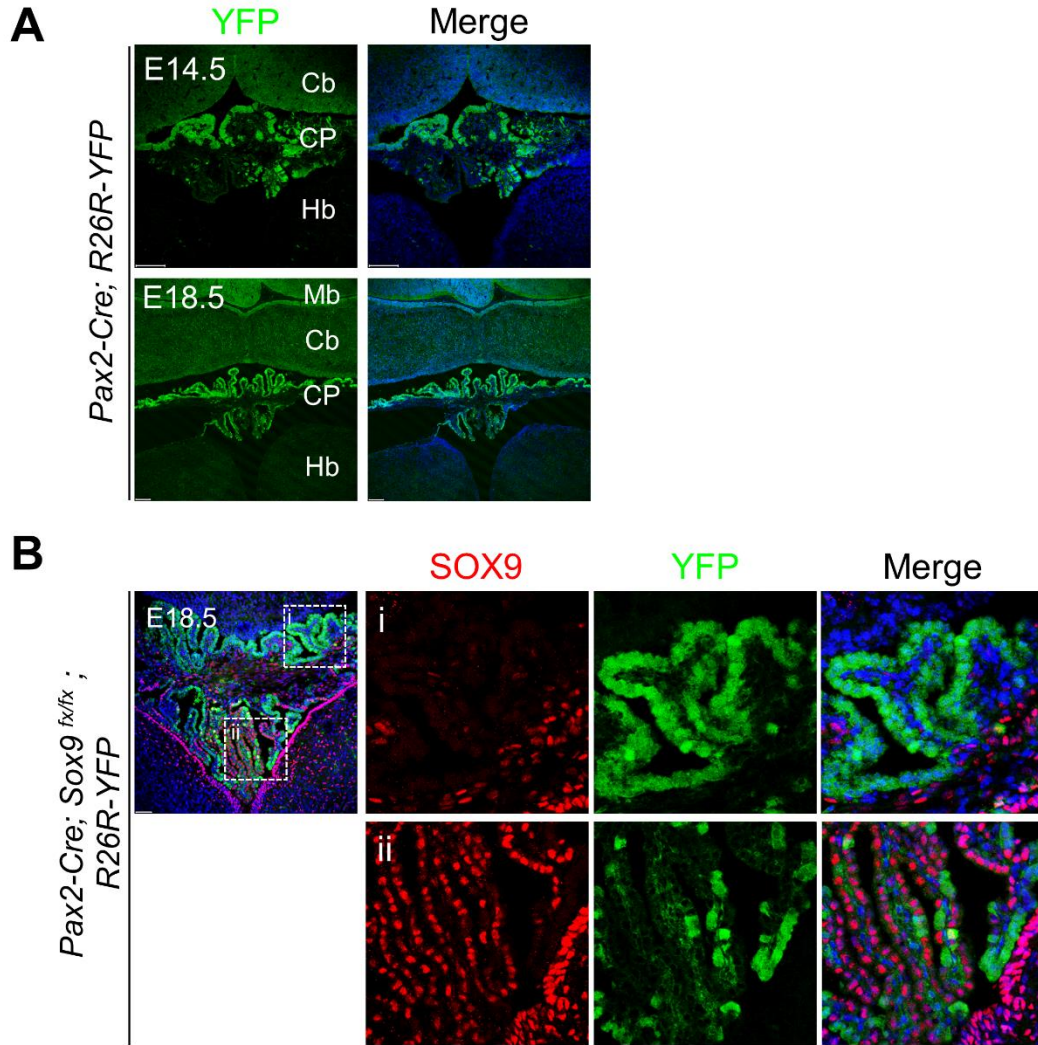
Fig. S2 *Pax2-Cre* mediated recombination in the hindbrain CP epithelium. (A) YFP labelled the midbrain (Mb), cerebellum (Cb) and hindbrain CP but not the hindbrain (Hb) of *Pax2-Cre; R26R-YFP* reporter mice at E14.5 and E18.5. (B) Immunostaining confirmed the removal of SOX9 from YFP$^+$ cells in the *Sox9* CKO CP epithelium. SOX9 expression was not affected in YFP$^-$ cells. Scale bars, 100 µm in A-B.
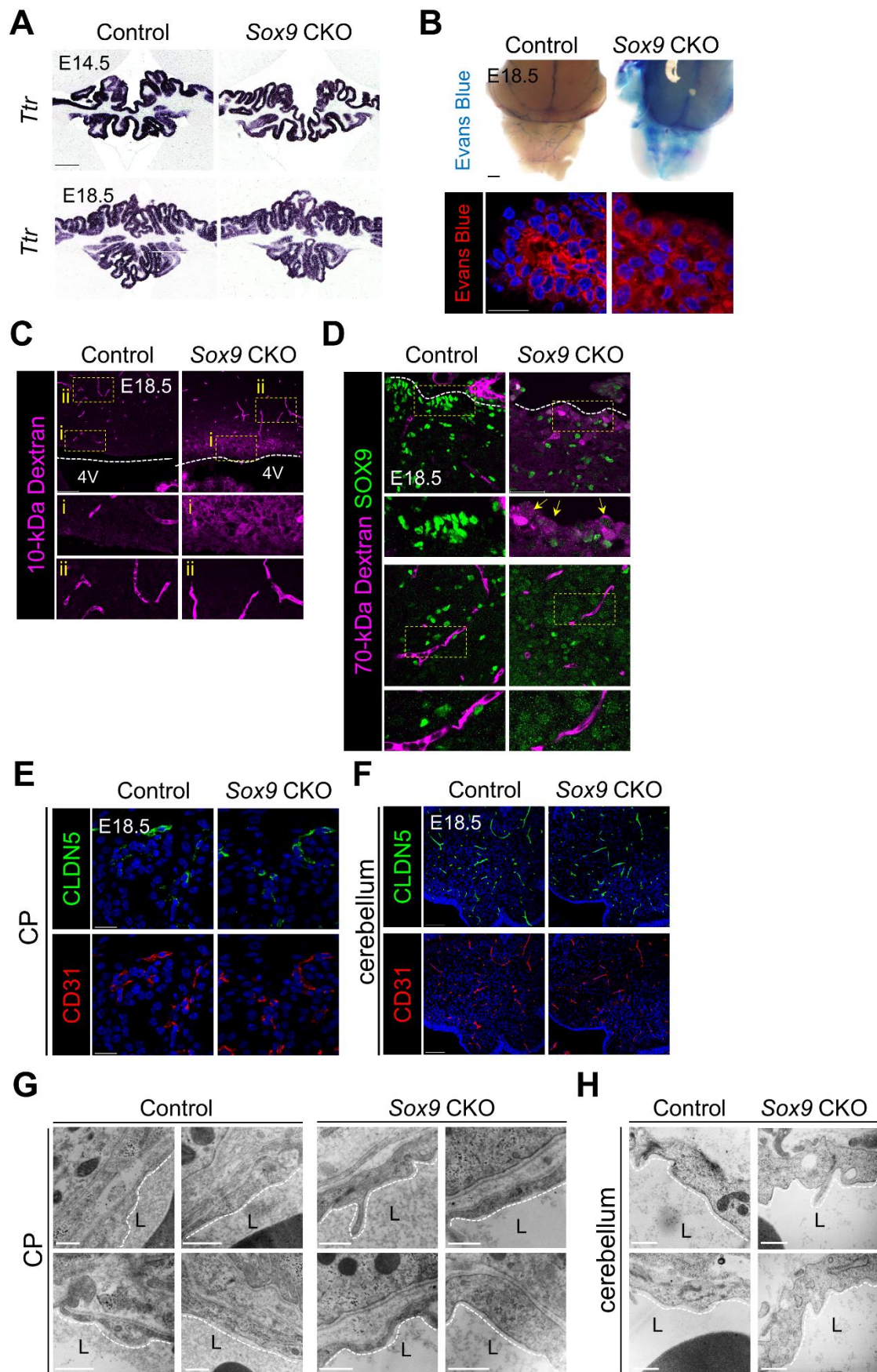
Fig. S3 Vasculature in CP or brain parenchyma were not affected in *Sox9* CKO. (A) *In situ* hybridization for detection of *Ttr* transcripts at E14.5 and E18.5 control and *Sox9* CKO CP. (B) Evans Blue extravasation assay revealed albumin leakage in the CP epithelium of *Sox9* CKO. *n*=3 per genotype. (C-D) Analysis of blood-CSF barrier permeability by *in utero* liver injection of rhodamine conjugated 10-kDa or 70-kDa dextran into E18.5 embryos. (C) 10-kDa dextran was excluded from the neural tissue in controls but entered the cerebellar ventricular zone of *Sox9* CKO mutants. (i) and (ii) are zoomed-in views of the corresponding boxes. (D) Similarly, 70-kDa dextran was restricted within the brain vessels but found adjacent to the ventricular surface (yellow arrows). (E-F) Immunostaining for CLDN5 or CD31 in sagittal sections from control and *Sox9* CKO at E18.5. The expression pattern of CLDN5 and CD31 in CP (E) and cerebellum (F) were not affected by conditional *Sox9* deletion. *n*=3 per genotype. (G-H) Transmission electron microscopy images showing the vascular endothelium in (G) CP and (H) cerebellum. White dotted lines outlined the endothelial cell wall. L, capillary lumen. *n*=2 per genotype. Scale bars, 50 µm in A, C, D and E, 20 µm in B, 100 µm in F, 500 nm in G-H.
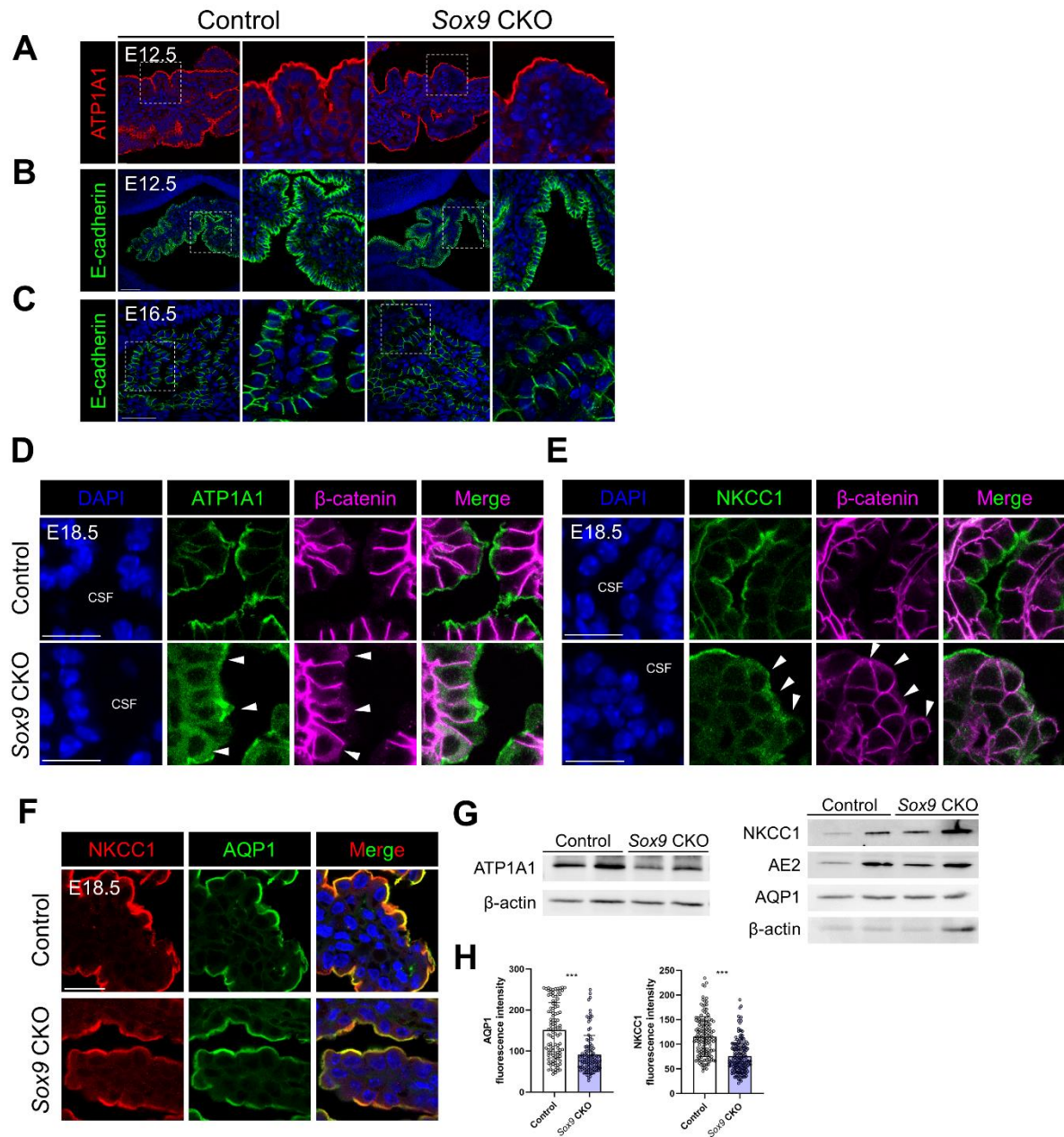
Fig. S4 Loss of epithelial polarity following *Sox9* deletion in the CP. (A) Representative images showing the immunofluorescence of ATP1A1 in CP at E12.5. (B-C) Immunostaining for E-cadherin on coronal sections of E12.5 (B) and E16.5 (C) control and *Sox9* CKO embryos. *n*=3 per genotype. (D-E) Double immunofluorescence staining for β-catenin and (D) ATP1A1 or (E) NKCC1 in CP at E18.5. Arrowheads indicated the incorrect orientation of transporters and polarity complexes in *Sox9* CKO CP. (F) Representative images showing the double immunofluorescence staining of NKCC1 and AQP1 in control or *Sox9* CKO CP at E18.5. (G) Immunoblots showing the abundance of ATP1A1, AE2, AQP1 and NKCC1 in control or *Sox9* CKO CP. (H) Quantification of AQP1 and NKCC1 fluorescent intensity at the apical surface. *n*>50 cells from at least 3 mice per genotype. Data are mean ± SEM. ***P<0.001. Scale bars, 20 µm in A, C, D and E, 50 µm in B, 10 µm in F.
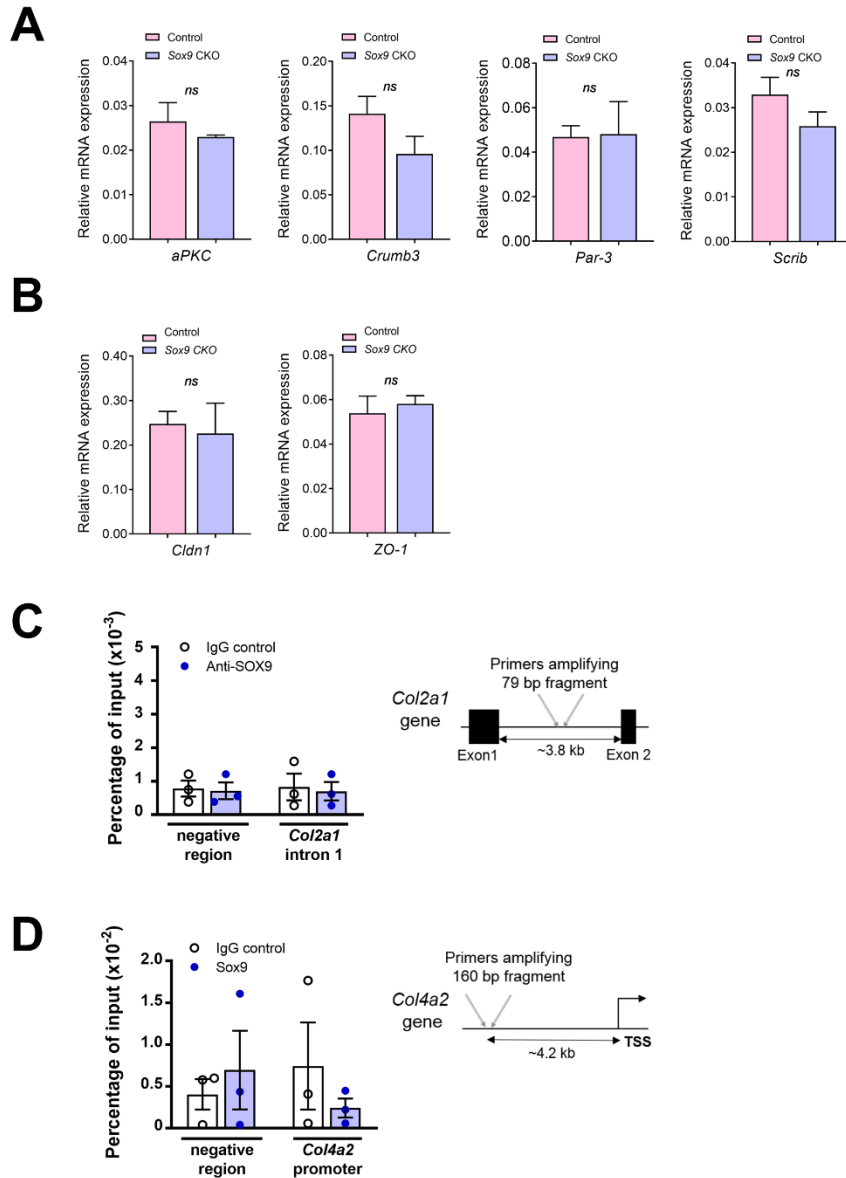
Fig. S5 Epithelial polarity was not transcriptionally regulated by SOX9. (A-B) Bar charts showing the relative mRNA level of genes involving in (A) cell polarity establishment (*aPKC*, *Crumb3*, *Par-3* and *Scrib*) and (B) tight junction assembly (*Cldn1* and *ZO-1*) in hindbrain CP of control and *Sox9* CKO embryos at E16.5. Data are mean ± SEM. *ns,* not statistically significant. (C-D) ChIP-qPCR analysis of SOX9 binding to (C) *Col2a1* intron 1 and (D) *Col4a2* enhancer approximately 4 kb upstream of the transcription start site. Non-targeting IgG was used as negative control. The binding occupancy was represented as % input. *n*=3 independent experiments. Data are mean ± SEM.
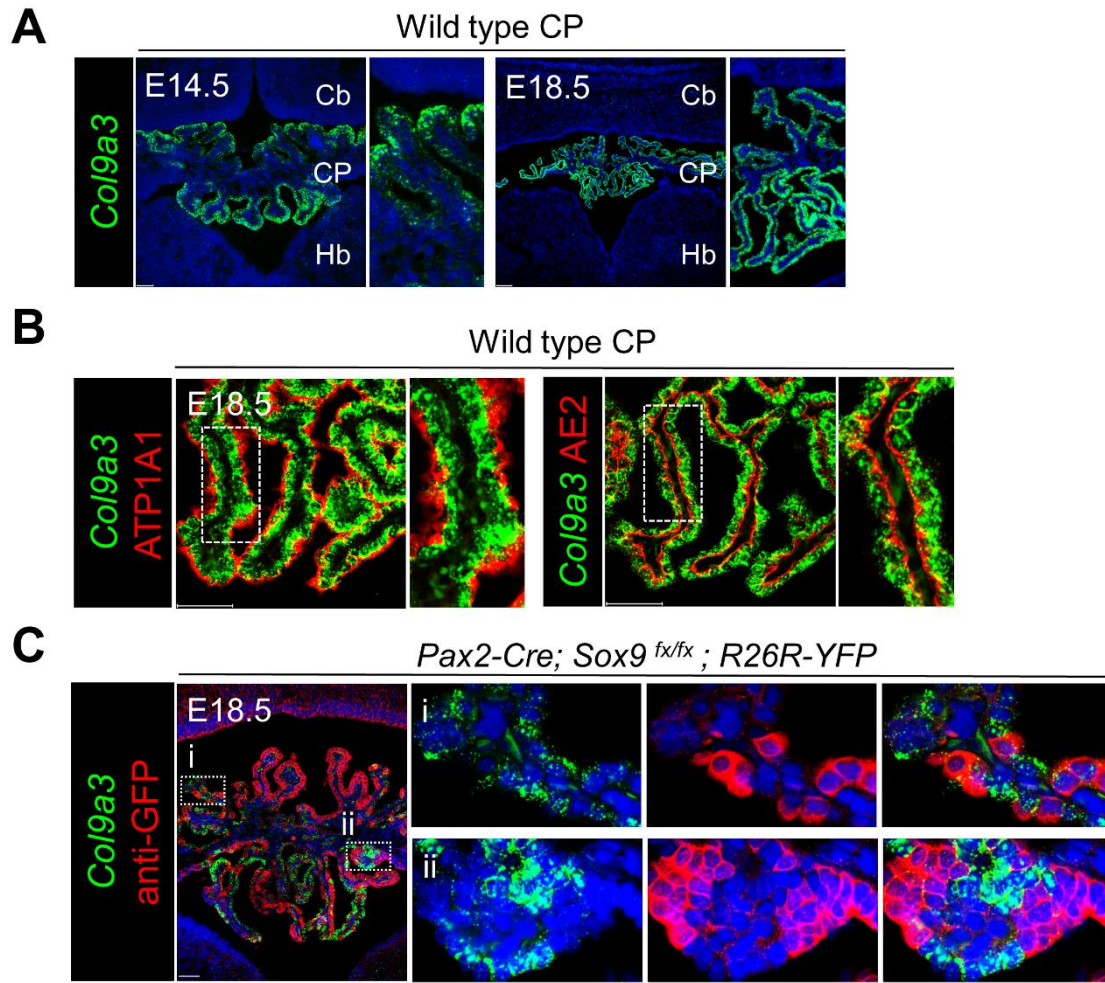
Fig. S6 *Col9a3* expression in the CP. (A) RNAscope *in situ* hybridization showing the expression pattern of *Col9a3* in coronal brain sections of the E14.5 and E18.5 mouse embryos. (B) RNAscope for *Col9a3* followed by immunostaining for ATP1A1 or AE2 in the E18.5 CP. (C) RNAscope for *Col9a3* followed by immunostaining for YFP using anti-GFP antibodies in sections from *Sox9* CKO mice carrying the *ROSA26-YFP* reporter allele. Cb, cerebellum. CP, choroid plexus. Hb, hindbrain. Scale bars, 100 μm in A and C, 20 μm in B.
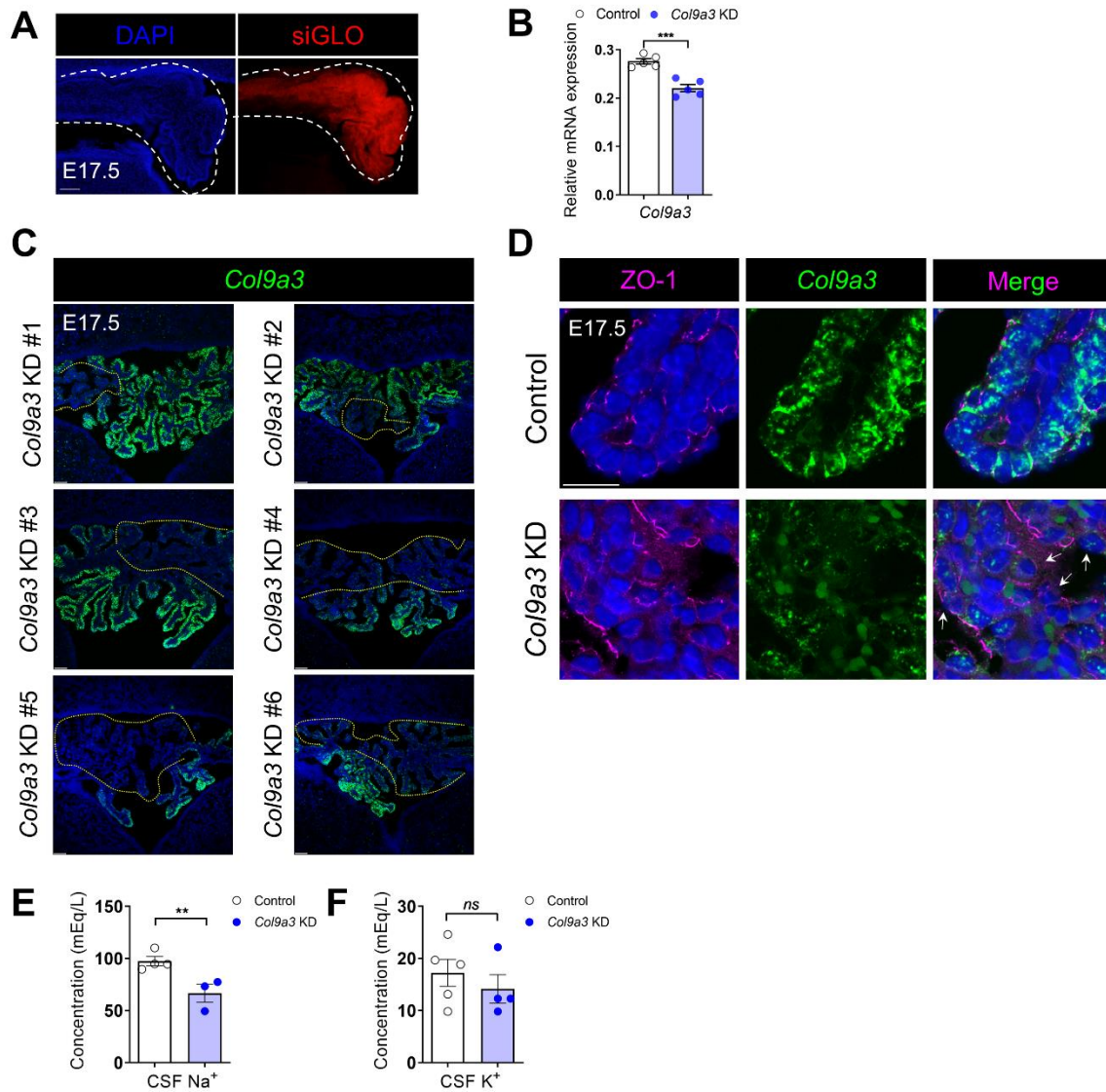
Fig. S7 Knockdown of *Col9a3* in the CP. (A) *In utero* electroporation of Cy5-conjugated non-targeting double stranded RNA (siGLO) into hindbrain CP at E14.5. Representative whole-mount image showing the transfection efficiency after electroporation. Dotted lines outline the CP. (B-C) The knockdown efficiency of *Col9a3* in CP was verified by RT-qPCR analysis (B) and RNAscope (C). (D) Immunostaining for ZO-1 3 days after *Col9a3* KD. *Col9a3* silenced cells were identified by RNAscope. (E-F) Analysis of Na^+ and K^+ concentrations in CSF from control and *Col9a3* KD mice by atomic absorption spectroscopy. Data are mean ± SEM. **$P<0.01$. ***$P<0.001$. *ns,* not statistically significant. Scale bars, 100 μm in A and C, 10 μm in D.
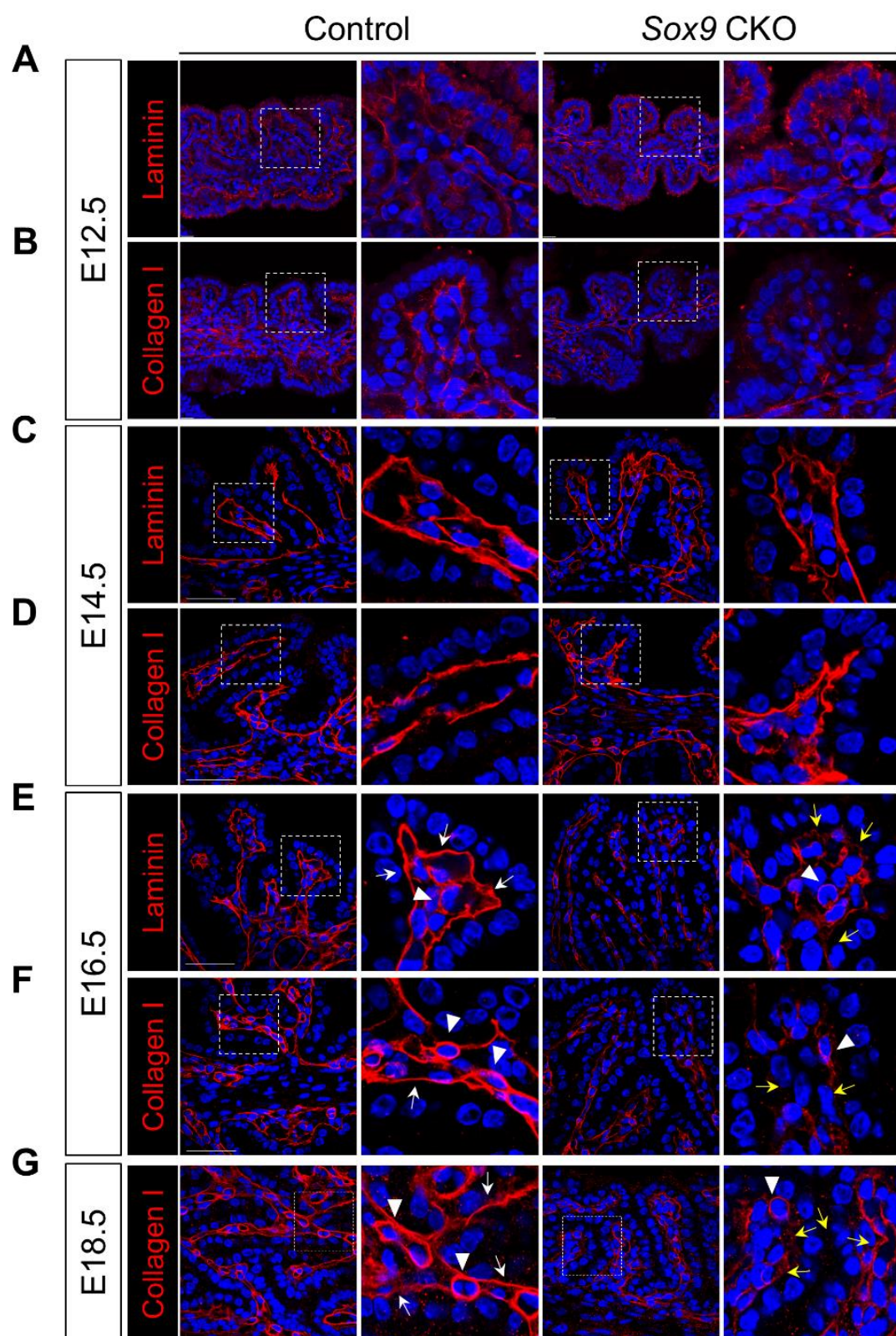
Fig. S8 Time course for the loss of ECM components at the epithelial basement membrane of the *Sox9* CKO mutant CP. (A-F) Representative images showing the expression of laminin

and collagen I in the hindbrain CP at E12.5 (A-B), E14.5 (C-D) and E16.5 (E-F). The subepithelial basement membrane (white arrows) was progressively deposited with laminin (A, C, E) and collagen I (B, D, F), which were apparently unaffected by *Sox9* deletion until after E16.5 (yellow arrows). (G) Immunostaining for collagen I on control and *Sox9* CKO mutant sections at E18.5. Filled arrowheads indicate vascular endothelium. Scale bars, 50 µm in A-G.
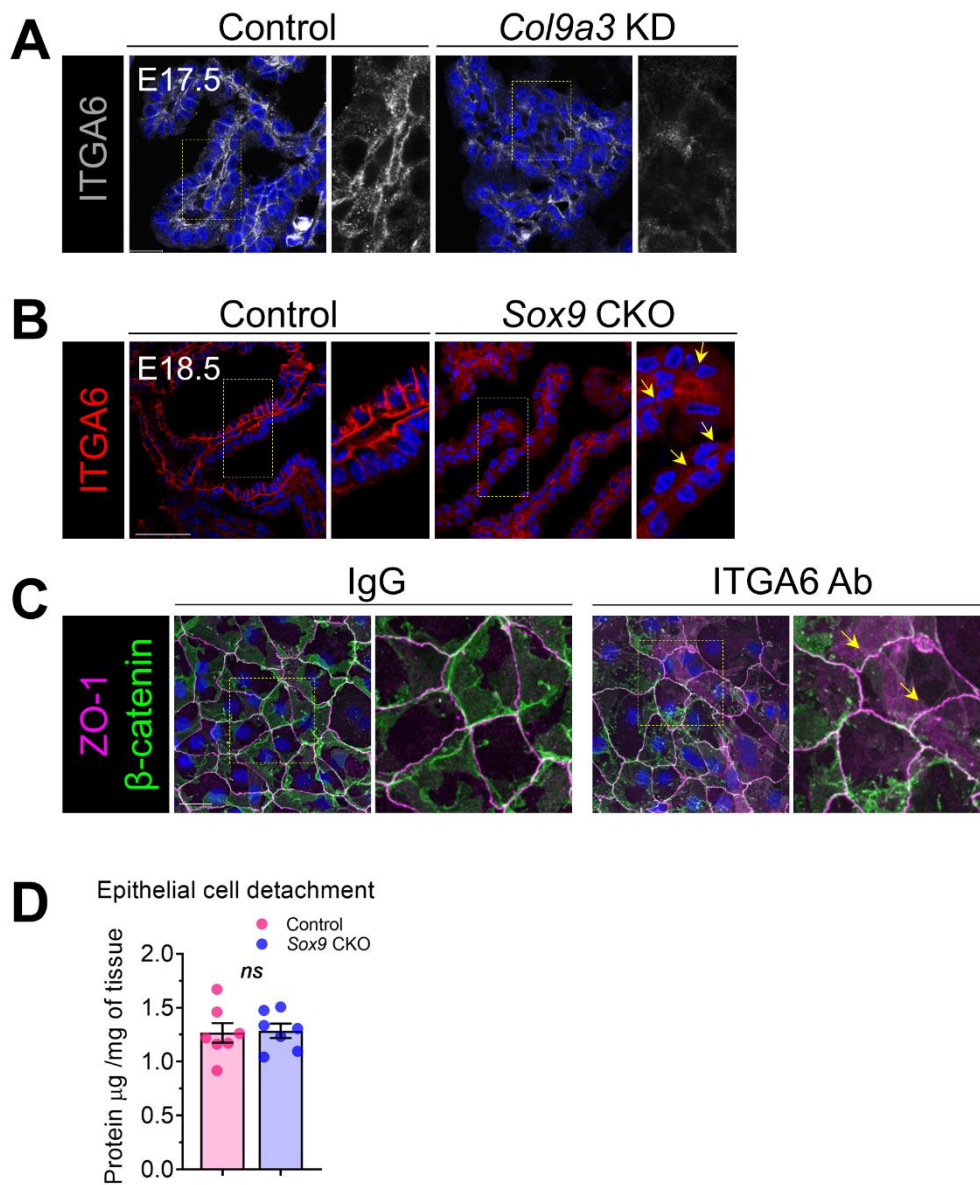
Fig. S9 Importance of ECM-integrin interactions in establishing apicobasal polarity. (A-B) Representative images showing the loss of integrin α6 (ITGA6) expression from CP upon (A) *Col9a3* KD or (B) *Sox9* CKO. (C) CP epithelial cells were treated with normal IgG or function-blocking ITGA6 antibody and cultured for 3 days *in vitro*. The subcellular localization of ZO-1 and β-catenin were determined by immunostaining. Arrows indicate the loss of apicobasal polarity. (D) No significant difference in the epithelial fragility between control and Sox9 mutant CP. *n*=3 independent experiments. Scale bars, 20 µm in A-C.

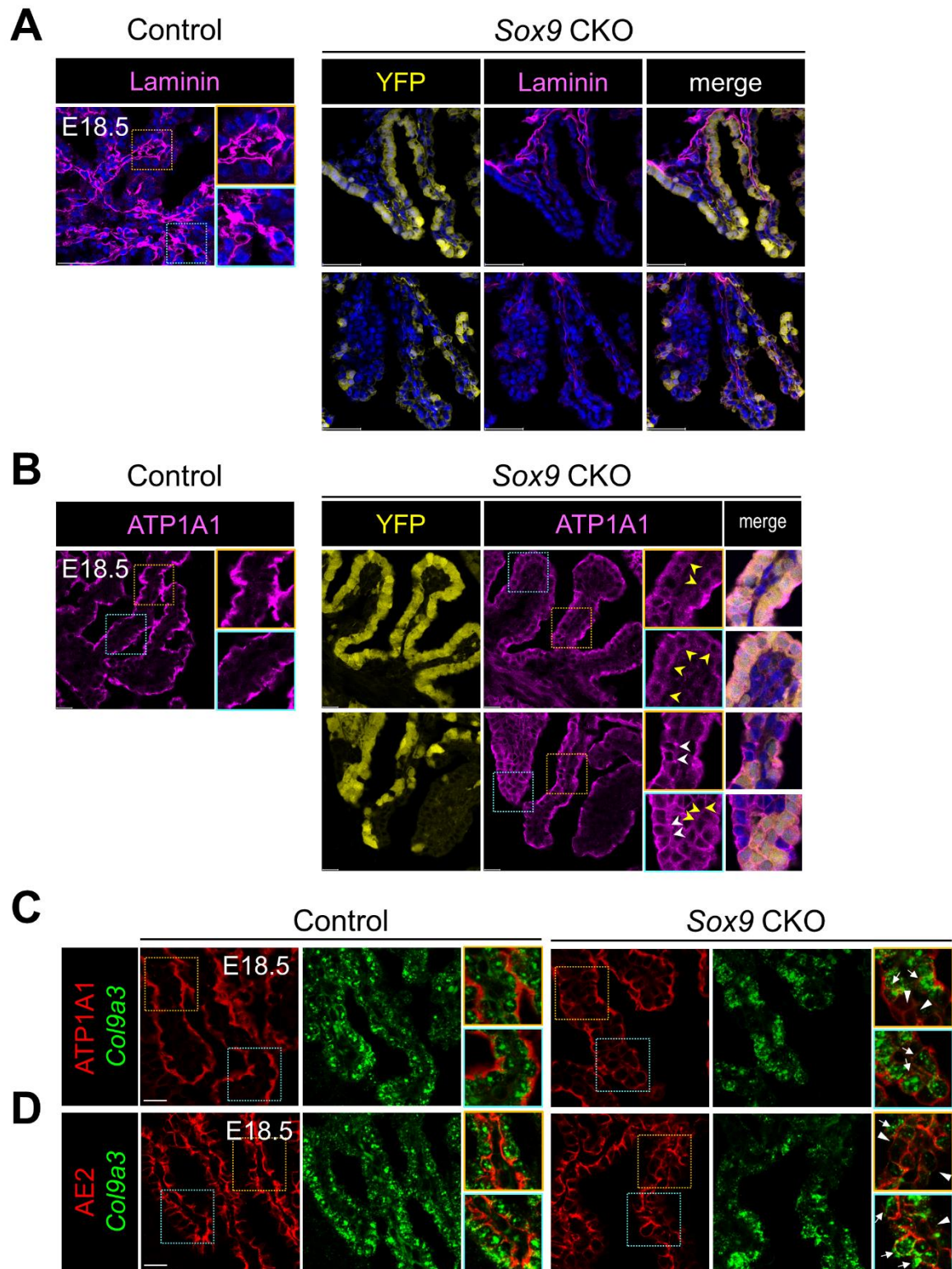**Fig. S10** Non-cell autonomous regulation of apicobasal polarity in the CP by SOX9. (A) Representative images of *R26R-YFP* expression and laminin immunostaining in control or *Sox9* CKO mutant. (B) Representative images of *R26R-YFP* expression and ATP1A1

immunostaining in control or *Sox9* CKO mutant. White and yellow arrows indicated YFP$^-$ and YFP$^+$ cells that showed altered polarization of ATP1A1 respectively. (C-D) Representative images showing RNAscope analysis of *Col9a3* expression followed by immunostaining for (C) ATP1A1 or (D) AE2 in E18.5 CP. Arrowheads indicated the *Col9a3*$^-$ CP epithelium in the *Sox9* CKO showing altered expression of the transporters. Arrows indicated the cells with misoriented transporters even in the presence of *Col9a3* expression. Scale bars, 50 μm in A, 20 μm in B-D.
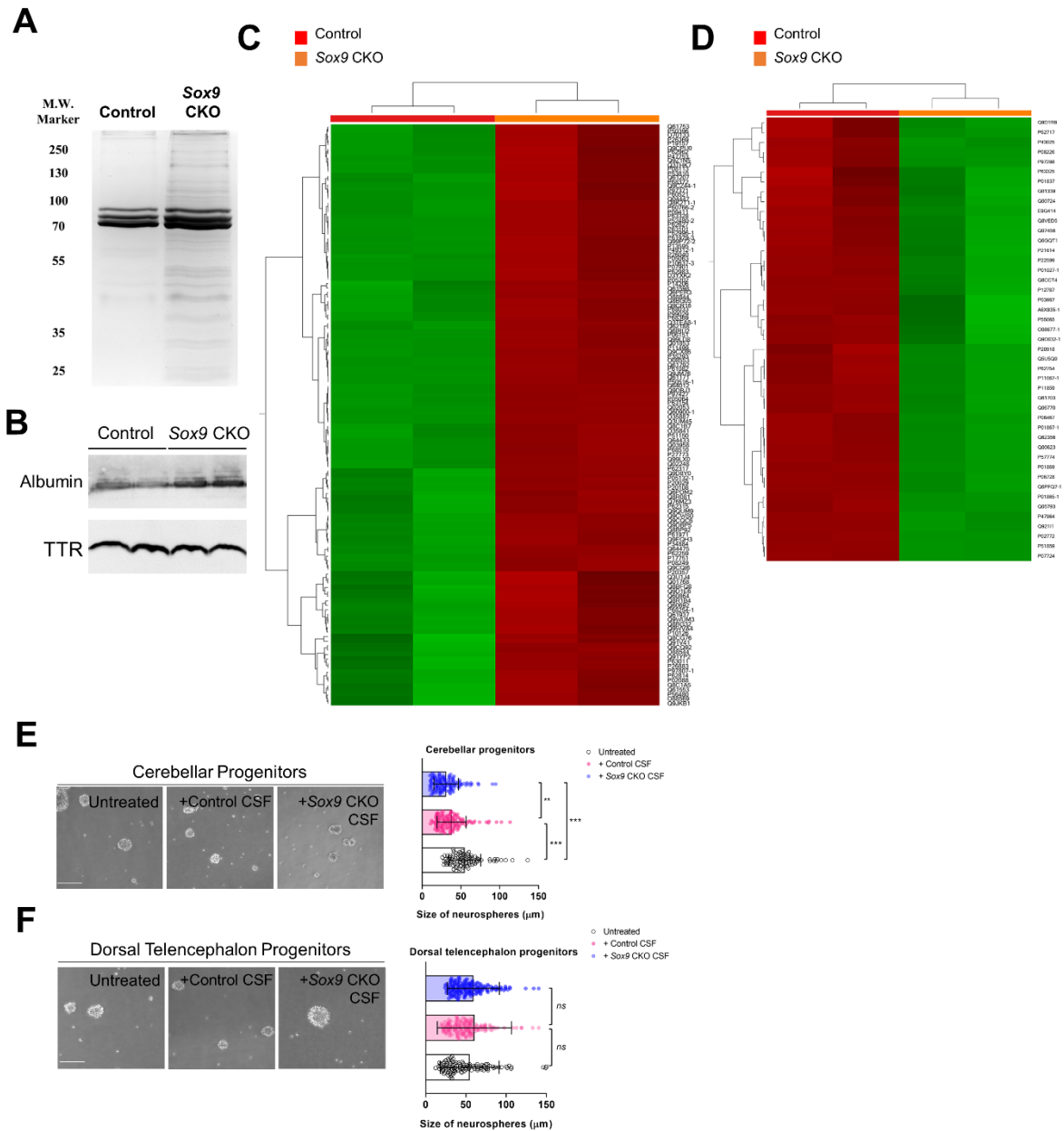
Fig. S11 CSF proteome was altered following *Sox9* deletion in the CP. (A) Silver staining of CSF proteins from control and *Sox9* CKO. Same volume of pooled CSF sample from control or *Sox9* CKO were separated by 10% SDS-PAGE gel. (B) Western blot showing the abundance of albumin and transthyretin (TTR) in CSF isolated from control or *Sox9* CKO. Same volume of pooled CSF was applied to the protein gel. (C-D) Heatmap showing the most enriched protein in CSF from (C) *Sox9* CKO or (D) control mice as revealed by LC-MS/MS. The green and red colors represent low and high relative abundance of proteins, respectively. The Uniprot accession numbers were shown in the right of each column of the heat map. (E-F) Dissociated neural progenitors from E14.5 (E) cerebellum or (F) dorsal telencephalon were cultured for 7 days with or without CSF from control or *Sox9* CKO

embryos. Scatter plots showing the size of neurospheres formed from (E) cerebellar and (F) dorsal telencephalon progenitors in each treatment group. $n=2$ independent experiments and $\geqq 50$ neurospheres were analyzed from each experiment. Data are mean ± SEM. **$P<0.01$. ***$P<0.001$. *ns,* not statistically significant. Scale bars, 50 µm in E and F.

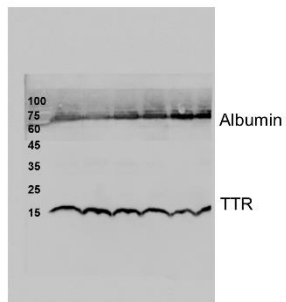Original blot image for Fig. S4G
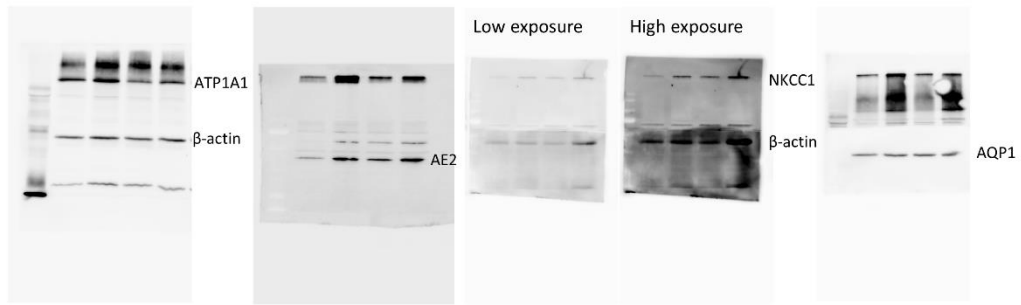
Original blot image for Fig. S10B

Fig. S12 Original immunoblot images of Fig. S4G and Fig. S10B.

Table S1 Change in expression level of ECM genes in *Sox9* CKO mutants at E16.5.

Gene symbol	Log$_2$ (Fold Change)	P value
Col1a1	0.182961	0.4264
Col1a2	0.061853	0.7976
Col2a1	-0.01085	0.9683
Col4a1	-0.0088	0.9722
Col4a2	-0.00058	0.9977
Col4a3	-0.26537	0.23965
Col4a4	-0.43694	0.06945
Col4a5	-0.13805	0.5192
Col5a1	0.188078	0.3982
Col9a1	-0.64713	1
Col9a2	-1.05133	5.00E-05
Col9a3	-1.37112	5.00E-05
Col10a1	-0.01532	1
Col11a1	0.237616	0.31445
Col11a2	-0.12737	0.7579
Col13a1	-0.3159	0.2075
Col14a1	-0.40922	0.0694
Col15a1	-0.01913	0.93095
Col16a1	0.345034	0.1311
Col17a1	-0.0657	1
Col18a1	0.22063	0.3214
Ecm1	-0.0408	0.88005
Fn1	0.287729	0.2488
Lama1	0.276277	0.36245
Lama2	-0.44944	0.04555
Lama3	0.109938	0.6879
Lama4	0.091559	0.6796
Lama5	0.059583	0.7919
Lamb1	-0.01816	0.9361
Lamb2	-0.03557	0.8682
Lamb3	-0.39739	1
Lamc1	0.061622	0.78525
Lamc2	0.553628	0.2034
Lamc3	-0.78032	0.0035

Mmp2	0.055629	0.7996
Mmp11	-0.1323	0.6467
Mmp14	0.047247	0.83105
Mmp15	0.091704	0.67715
Mmp16	0.194331	0.4778
Mmp17	0.49275	0.36745
Mmp19	0.515527	0.3824
Postn	0.13795	0.5383
Vcan	-0.16056	0.48905
Vtn	-0.10636	0.67345

Table S2 List of proteins with differential abundance in the CSF from *Sox9* CKO mutants

Top 20 less-abundant proteins in the CSF of *Sox9* CKO					
Protein name	**Accession number**	**MW**	**Calc. pI**	**Abundance**	**Adjusted *p* value**
Alpha-fetoprotein	P02772	67.3	5.92	0.521	6.18E-11
Ras GTPase-activating protein 4	Q6PFQ7-1	90.0	8.00	0.524	0.002131
Keratin, type II cytoskeletal 79	Q8VED5	57.5	7.69	0.527	0.006485
corticosteroid-binding globulin	Q06770	44.7	5.24	0.527	0.002278
Apolipoprotein A-IV	P06728	45	5.47	0.563	0.001378
Apolipoprotein A-II	P09813	11.3	7.18	0.575	0.002295
Collagen alpha-1(V) chain	O88207	183.6	4.98	0.583	0.004785
Serum albumin	P07724	68.6	6.07	0.592	6.18E-11
Protein FAM3C	Q91VU0	24.7	8.29	0.611	0.018627
Heparin cofactor 2	P49182	54.	7.34	0.612	0.037766
Collagen alpha-1(I) chain	P11087-1	137.9	5.85	0.617	0.016222
Serotransferrin	Q921I1	76.7	7.18	0.621	2.05E-05
Basement membrane-specific heparan sulfate proteoglycan core protein	Q05793	398	6.32	0.626	2.99E-05
Prostaglandin-H2 D-isomerase	O09114	21.1	8.25	0.627	0.010721
Gelsolin	P13020-1	85.9	6.1	0.639	0.002589
Inter-alpha-trypsin inhibitor heavy chain H2	Q61703	105.9	7.27	0.639	0.002278
Fibrinogen gamma chain	Q8VCM7	49.4	5.86	0.644	0.019368
Ig gamma-2A chain C region, membrane-bound form	P01865-1	43.9	6.29	0.647	0.002295
Insulin-like growth factor-binding protein 2	P47877	32.8	7.64	0.654	0.035683
apolipoprotein B-100	E9Q414	509.1	6.81	0.656	0.003605
Top 20 over-abundant proteins in the CSF of *Sox9* CKO					
Protein name	**Accession number**	**MW**	**Calc. pI**	**Abundance**	**Adjusted *p* value**
Small nuclear ribonucleoprotein Sm D2	P62317	13.5	9.91	1.670	0.004757
Calretinin	Q08331	31.4	5.02	1.601	0.00205
Heterogeneous nuclear ribonucleoprotein K	P61979	50.9	5.54	1.510	0.007543

Neuromodulin	P06837	23.6	4.73	1.501	0.01652
poly(U)-binding-splicing factor PUF60	Q3UEB3	60.2	5.29	1.501	0.02528
Serine/arginine-rich splicing factor 3	P84104-1	19.3	11.65	1.489	0.003493
Actin, alpha cardiac muscle 1	P68033	42	5.39	1.473	0.001431
Cytochrome c, somatic	P62897	11.6	9.58	1.419	0.005196
Isoform Tau-B of Microtubule-associated protein tau	P10637-3	38.2	9.33	1.410	0.002589
Dihydropyrimidinase-related protein 2	O08553	62.2	6.38	1.397	0.000157
Actin-related protein 2/3 complex subunit 3	Q9JM76	20.5	8.59	1.387	0.000157
MARCKS-related protein	P28667	20.3	4.61	1.387	0.013007
L-lactate dehydrogenase A chain	P06151	36.5	7.74	1.385	0.0007100
LIM and SH3 domain protein 1	Q61792	30	7.05	1.375	0.007068
Serine/threonine-protein phosphatase 2B catalytic subunit alpha isoform	P63328	58.6	5.86	1.373	0.005108
Heat shock protein HSP 90-alpha	P07901	84.7	5.01	1.362	0.002511
Myristoylated alanine-rich C-kinase substrate	P26645	29.6	4.34	1.362	0.037429
lactoylglutathione lyase	Q9CPU0	20.8	5.47	1.355	0.005581
Dihydropyrimidinase-related protein 1	P97427	62.1	7.12	1.319	1.39E-05
Crooked neck-like protein 1	P63154	83.4	6.93	1.311	6.18E-11

Table S3 List of primers used in this study

Target Gene		Sequence (5' → 3')	Purpose
Actb	Forward	GGCTGTATTCCCCTCCATCG	RT-qPCR
	Reverse	CCAGTTGGTAACAATGCCATGT	
Col2a1	Forward	TGAAACCCTGCCCGTATTTATT	ChIP-qPCR
	Reverse	GCTTTTCTCAAGCGCATACAGA	
Col2a1	Forward	GGGGCGCTTTGTATGAAAGG	ChIP-qPCR
	Reverse	GTGAGCCAGTCTGGGTTTGA	(negative control)
Col4a2	Forward	TGACCTTTCATTGTGTGCTGGAC	ChIP-qPCR
	Reverse	GGTTTGGCATTTGGAACTCCG	
Col4a2	Forward	TCCACAGTTGGTGAAGGATTGGGC	ChIP-qPCR
	Reverse	CACAGGTCAAACTCCTCTAGTCC	(negative control)
Col9a2	Forward	AAGGGGCCTCCAGGTAAAGTT	RT-qPCR
	Reverse	TCCCATTAAACCATCAATGCCA	
Col9a2	Forward	GGGATCTGGAGAGATGGCTCCCTGC	ChIP-qPCR
	Reverse	TCTCCCAAGCATCCACCAGGCATC	
Col9a2	Forward	GTTTCTAATTTCAAGCACTATTAACA	ChIP-qPCR
	Reverse	CTTTCTTGCCACACCAATCAGGAAT	(negative control)
Col9a3	Forward	CAAGGATGGCATTGATGGAG	RT-qPCR
	Reverse	CAGACCATCTACACCAGGCAGT	
Col9a3	Forward	GAAGCCTTGCCATGGTAGGCTTTG	ChIP-qPCR
	Reverse	GCAACATTTTCTGGCCCTCCTCTTG	
Col9a3	Forward	TTAGACTCTGTCACCAGTTCTGTG	ChIP-qPCR
	Reverse	GCTGTGTTGGTGCTGGGAATTGAA	(negative control)
aPKC	Forward	GCGTGGATGCCATGACAAC	RT-qPCR
	Reverse	AATGATGAGCACTTCGTCCCT	
Cldn1	Forward	GGGGACAACATCGTGACCG	RT-qPCR
	Reverse	AGGAGTCGAAGACTTTGCACT	
Crumb3	Forward	CACCGGACCCTTTCACAAATA	RT-qPCR
	Reverse	CCCACTGCTATAAGGAGGACT	
Par-3	Forward	CGGATGATGTCTTAGCAGATGTT	RT-qPCR

	Reverse	CAGCCACTTCTGTCTCGAAAG	
Scrib	Forward	GGGGTGATCCAGCCATTGG	RT-qPCR
	Reverse	GGCCCTATACGCCTGCTTC	
ZO-1	Forward	GCCGCTAAGAGCACAGCAA	RT-qPCR
	Reverse	TCCCCACTCTGAAAATGAGGA	

References

1. A. D. Grimaldi, M. Fomicheva, I. Kaverina, Ice recovery assay for detection of Golgi-derived microtubules. *Methods Cell Biol* **118**, 401-415 (2013).

2. Y. Campos *et al.*, Alix-mediated assembly of the actomyosin-tight junction polarity complex preserves epithelial polarity and epithelial barrier. *Nat Commun* **7**, 11876 (2016).

3. A. M. Bolger, M. Lohse, B. Usadel, Trimmomatic: a flexible trimmer for Illumina sequence data. *Bioinformatics* **30**, 2114-2120 (2014).

4. C. Trapnell *et al.*, Differential gene and transcript expression analysis of RNA-seq experiments with TopHat and Cufflinks. *Nat Protoc* **7**, 562-578 (2012).